

# Design, Assembly, and Activity of Antisense DNA Nanostructures

Jung-Won Keum, Jin-Ho Ahn, and Harry Bermudez\*

*Discrete DNA nanostructures allow simultaneous features not possible with traditional DNA forms: encapsulation of cargo, display of multiple ligands, and resistance to enzymatic digestion. These properties suggested using DNA nanostructures as a delivery platform. Here, DNA pyramids displaying antisense motifs are shown to be able to specifically degrade mRNA and inhibit protein expression in vitro, and they show improved cell uptake and gene silencing when compared to linear DNA. Furthermore, the activity of these pyramids can be regulated by the introduction of an appropriate complementary strand. These results highlight the versatility of DNA nanostructures as functional devices.*

## 1. Introduction

DNA is an excellent material for supramolecular assembly due to its highly specific interactions,<sup>[1]</sup> enabling the creation of numerous intricate structures and devices.<sup>[2]</sup> In addition, DNA has well-known functional roles in biological settings, including the actions of DNAzymes and aptamers.<sup>[3]</sup> DNA nanostructures are therefore positioned to have significant utility in the field of nanomedicine. Additional benefits arise from the nanoscale properties of DNA: we previously reported the enhanced stability of a DNA tetrahedron to both specific and nonspecific enzymatic digestion,<sup>[4]</sup> due to steric hindrance and the rigidity of DNA at nanometer length scales.<sup>[5]</sup> Together with their ability to display multiple ligands,<sup>[6]</sup> encapsulate cargo,<sup>[7]</sup> and reconfigure their shapes,<sup>[8]</sup>

the enhanced stability of DNA nanostructures provided initial evidence that they might prove effective as delivery vehicles, beyond what is possible with traditional DNA forms. Herein we describe the design, construction, and evaluation of DNA nanostructures with antisense features. Our modular approach allowed us to integrate antisense functionality into our scaffold, and should permit the introduction of other bioactive functionalities such as DNAzymes. The successful in vitro down-regulation of two distinct targets bodes well for other uses of DNA nanostructures as rationally designed biomaterials.

## 2. Results and Discussion

The design of our antisense DNA pyramid builds upon previous work from our group and others,<sup>[9–4]</sup> and is assembled from five unique oligonucleotides (**Figure 1**). The edges of the pyramid are 20 base pairs (bp) or ~7 nm in length and are double-stranded DNA (dsDNA), with the exception of one edge, which displays a single-stranded DNA (ssDNA) loop (Figure 1a). This ssDNA loop encodes an antisense sequence, and thus endows the pyramid with the therapeutic functionality to down-regulate specific gene expression. Once the architecture of the loop-displaying DNA pyramid was specified, the sequence of each strand was generated with the Tiamat software.<sup>[10]</sup> The DNA nanostructure was formed in a one-pot assembly with rapid step-wise cooling and verified by native polyacrylamide gel electrophoresis, dynamic light scattering (DLS), and transmission electron microscopy (TEM).

J.-W. Keum<sup>[+]</sup>

Department of Chemical Engineering  
University of Massachusetts  
Amherst, MA 01003, USA

Dr. J.-H. Ahn<sup>[+]</sup>

Department of Chemical Engineering  
Massachusetts Institute of Technology  
Cambridge, MA 02139, USA

Prof. H. Bermudez

Department of Polymer Science and Engineering  
University of Massachusetts  
Amherst, MA 01003, USA

E-mail: bermudez@polysci.umass.edu

[+] This authors contributed equally to this work.

DOI: 10.1002/sml.201101804

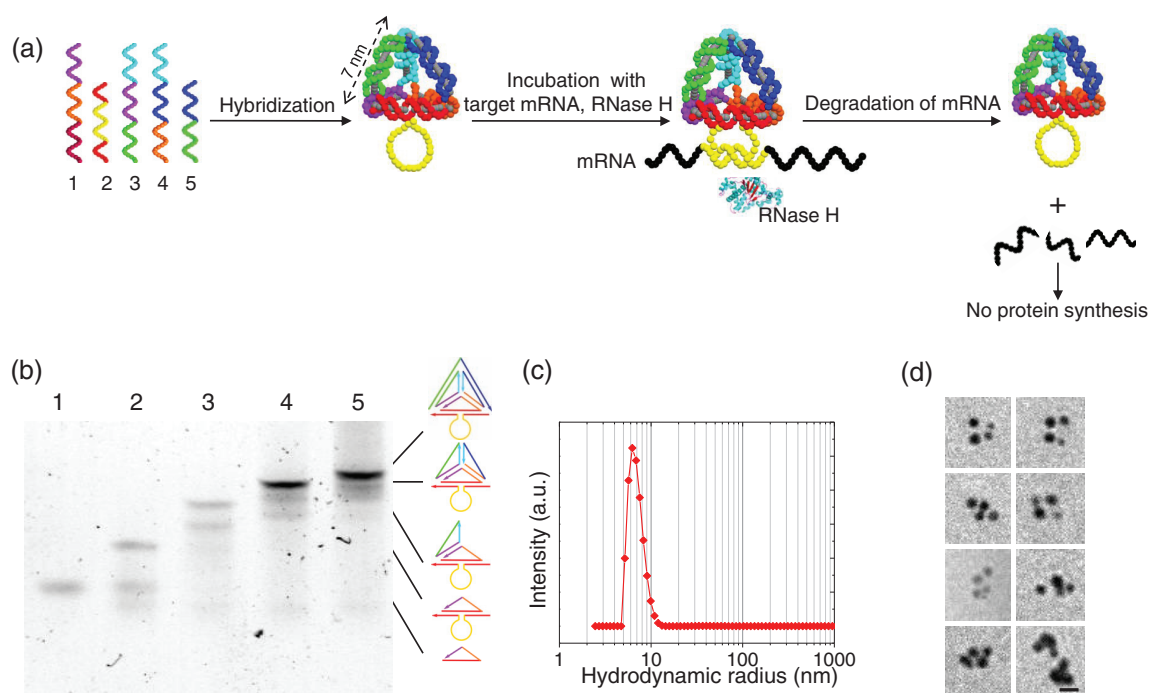


**Figure 1.** Design of antisense pyramid, its assembly, and characterization. a) Five oligonucleotides were assembled to form a pyramid with an ssDNA antisense loop (shown in yellow). Subsequent incubation with target mRNA and RNase H leads to specific digestion of target mRNA. b) Native polyacrylamide gel electrophoresis (PAGE) to verify assembly of the antisense pyramid, with the presumed structures schematically indicated to the right of the gel. Lane 1: strand 1; Lane 2: strand 1 and strand 2; Lane 3: strands 1–3; Lane 4: strands 1–4; Lane 5: strands 1–5. c) DLS results indicate a mean hydrodynamic size of  $6.0 \pm 1.0$  nm. d) TEM images of antisense pyramid–gold nanoparticle conjugates. Clusters of four particles are visible with an interparticle spacing of  $7.6 \pm 0.6$  nm. Scale bar corresponds to 5 nm.

Native gel electrophoresis (Figure 1b) shows that when all five strands are present, a distinct band with low mobility (i.e., high molecular weight) is present, indicating the formation of the intended structure. The efficiency of assembly was calculated to be 86%, by following the procedure of Goodman et al.<sup>[9]</sup> DLS revealed that the population has a mean hydrodynamic radius of  $6.0 \pm 1.0$  nm (Figure 1c), which corresponds well with that of a sphere circumscribed about our nanostructure. To obtain TEM imaging (Figure 1d), four of the five strands were thiol-modified and mixed with 2 nm gold nanoparticles so that a pyramid could recruit one gold nanoparticle at each vertex.<sup>[11]</sup> As a result, it could be directly observed that the distance between four gold nanoparticles was  $7.6 \pm 0.6$  nm, consistent with the successful assembly of pyramids.

The ssDNA loop in strand 2 was designed to contain a 20-nucleotide antisense sequence (Figure 1a), so as to eventually form a DNA–RNA heteroduplex with the target mRNA. We note that hybridization of as little as 6 nucleotides (out of the 20) can be used to trigger RNase H-mediated degradation,<sup>[12]</sup> leaving the antisense DNA strand intact.<sup>[13]</sup> The target mRNA was chosen to be the 312–331 region of enhanced green fluorescent protein (EGFP), as determined by the Sfold program<sup>[14]</sup> and previous evaluation in a cell-free protein synthesis system.<sup>[15]</sup> To test if our DNA pyramids could trigger RNase H-mediated gene silencing as designed, we examined mRNA levels and subsequent protein expression in a cell-free protein synthesis mixture. Such cell-free

systems are particularly useful for assessing antisense activity, independent of complicating intracellular effects.<sup>[16]</sup> In this approach, template DNA is incubated with the cell-free protein synthesis mixture and any of the various treatments to be compared. Successful down-regulation is reflected in lower levels of both mRNA and protein. As shown in **Figure 2a**, rapid degradation of EGFP mRNA was observed in the presence of antisense pyramids. Importantly, there is a stable level of 16S ribosomal RNA irrespective of treatment. There was also no degradation by antisense pyramids when using different templates (TNF- $\alpha$ , EGF, IL2, bGFP, DHFR) which indicates sequence specificity and no appreciable off-target effects of antisense pyramid (Figure S1, Supporting Information (SI)). When protein levels were evaluated in the cell-free system, incubation with the antisense pyramid suppresses protein synthesis to nearly the same extent as the ssDNA antisense alone (Figure 2b), due to the degradation of the corresponding mRNA (Figure 2a). Control experiments with EGFP template alone, and template plus control DNA, gave the expected protein synthesis. The fluorescence data of Figure 2b was independently confirmed by sodium dodecyl sulfate (SDS)-PAGE analysis (Figure S2, SI). The ability to specifically trigger both mRNA degradation and protein down-regulation, shown here, are important steps in establishing DNA nanostructures as potential antisense delivery vehicles.

The ssDNA antisense loop of the pyramid additionally provides a mechanism for regulation. Specifically, a DNA

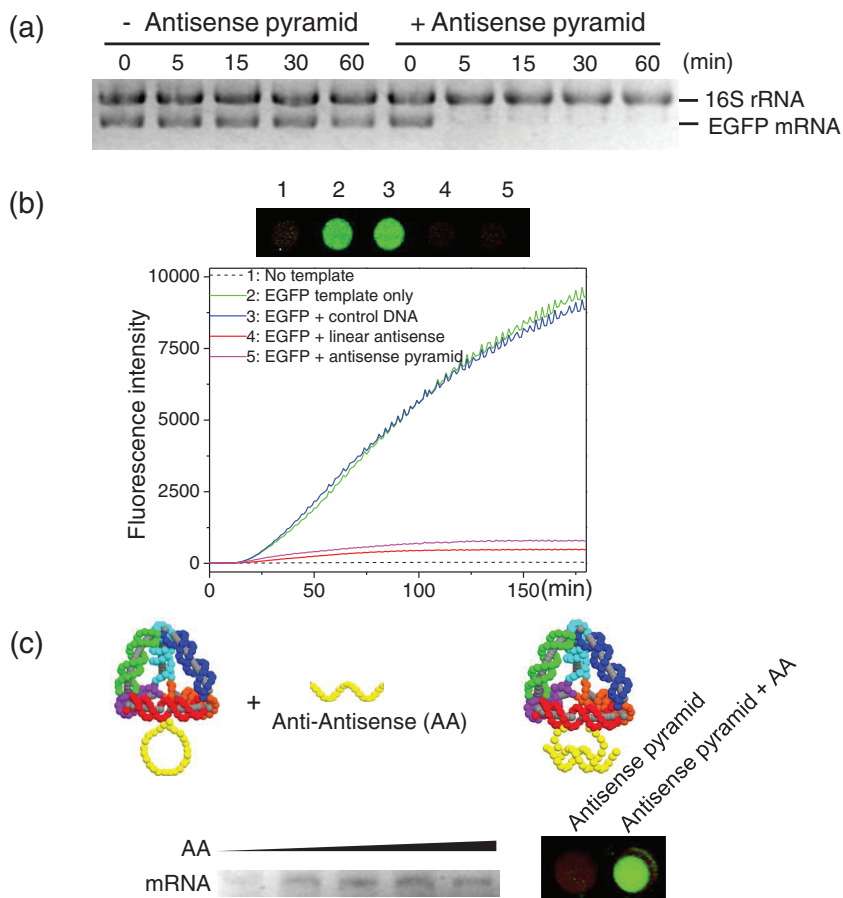


**Figure 2.** In vitro demonstration of the specific activity of antisense pyramids. a) Analysis of mRNA transcripts in the cell-free reaction with EGFP template. b) Real-time fluorescence of EGFP in a cell-free translation system. The absence or presence of each DNA type is shown in the legend. On the top is a corresponding fluorescence image after completion of the reaction. c) Incubation with an “anti-antisense” strand (complementary to the antisense loop) turns off the activity of antisense pyramid in a competitive manner. Molar excess of the anti-antisense relative to pyramid increases from 0, 1 $\times$ , 3 $\times$ , 6 $\times$ , and 9 $\times$  in the gel lanes from left to right.

strand that is complementary to the antisense loop will compete with the target mRNA strand for hybridization, shifting the equilibrium away from DNA–RNA heteroduplexes. Since DNA–RNA heteroduplexes are the substrates for RNase H, any reduction in heteroduplex concentration will effectively inhibit antisense activity. We proceeded to test this mechanism of competitive regulation by adding such a complementary DNA strand, denoted as anti-antisense (AA). The strength of the competing interaction was kept constant (i.e., the AA strand is 20 nucleotides (nt) in length), and the molar excess of anti-antisense was used to shift the equilibrium away from DNA–RNA heteroduplexes and towards DNA–DNA duplexes. Regulation was monitored by both EGFP mRNA levels and EGFP protein synthesis (Figure 2c). With increasing excess of the anti-antisense strand, mRNA levels were restored and EGFP expression was recovered in the cell-free reaction mixture. Thus the activity of these antisense pyramids can be reversibly regulated by the addition of an external strand. To determine whether the antisense strand remains within the nanostructure upon hybridization with its target, we examined the structure before and after

incubation with the AA strand by gel electrophoresis (Figure S3, SI). At equimolar concentrations of AA, the antisense strand is released from the pyramid, suggesting that the mRNA target is also capable of “extracting” the antisense strand from the pyramid. Of course, the ratio of loop-to-arm length in the pyramid can be altered to shift the equilibrium as desired. In contrast to simpler DNA forms, the pyramids are more structurally robust to perturbations by external strands<sup>[17]</sup> and temperature.<sup>[18]</sup> Given our interest in cellular delivery, this robustness is a key advantage.

The above results motivated cellular uptake experiments, and thus the antisense strand (strand 2) was modified with a Cy5 dye at its 3'-end to allow for fluorescence visualization. Initial experiments revealed minimal cell uptake for both pyramids and linear dsDNA controls, likely due to repulsive electrostatic interactions at the cell surface.<sup>[19]</sup> In order to attenuate the charge density, we therefore mixed pyramid and control samples with cationic lipofectamine. The resulting complexes were incubated with both human cervical carcinoma (HeLa) and mouse myoblast (C2C12) cells in serum-supplemented culture medium. The serum concentration in the culture medium was varied to examine the role of degradation on cell uptake efficiency. Cell uptake after 5 h was quantitatively assessed using flow cytometry, with appropriate controls (Figure 3a,b). Since five out of six edges of our pyramids are double-stranded, we compared uptake of pyramids against linear dsDNA. Using

other DNA forms as controls (e.g., partial duplex) did not give substantially different results (Figure S4, SI). We did not compare uptake against circular DNA since our pyramid is not ligated. As expected, with increasing serum concentration, cell uptake is reduced for both pyramid and linear forms, due to degradation by nucleases.<sup>[20]</sup> However, pyramids always showed higher cell uptake than the corresponding linear dsDNA forms. Given the above differences, it appears that the pyramids maintain some degree of their original structure, despite the use of lipofectamine.

Taking the ratio of pyramid uptake to linear uptake as an “enhancement factor”  $\epsilon$ , it is seen that  $\epsilon$  increases with serum concentration, reaching a plateau value of  $\epsilon \approx 3$  at 5–10% serum for both cell lines. The increased uptake of the pyramid appears to be a consequence of the enhanced stability in the presence of nucleases, as demonstrated in Figure 3c and supported by our previous work.<sup>[4]</sup> Indeed, the nanoscale dimensions and non-native geometries of antisense pyramids might have been predicted to resist enzymatic digestion more readily than their linear counterparts.<sup>[21–23]</sup> We note that the improved serum stability of our DNA pyramids does not

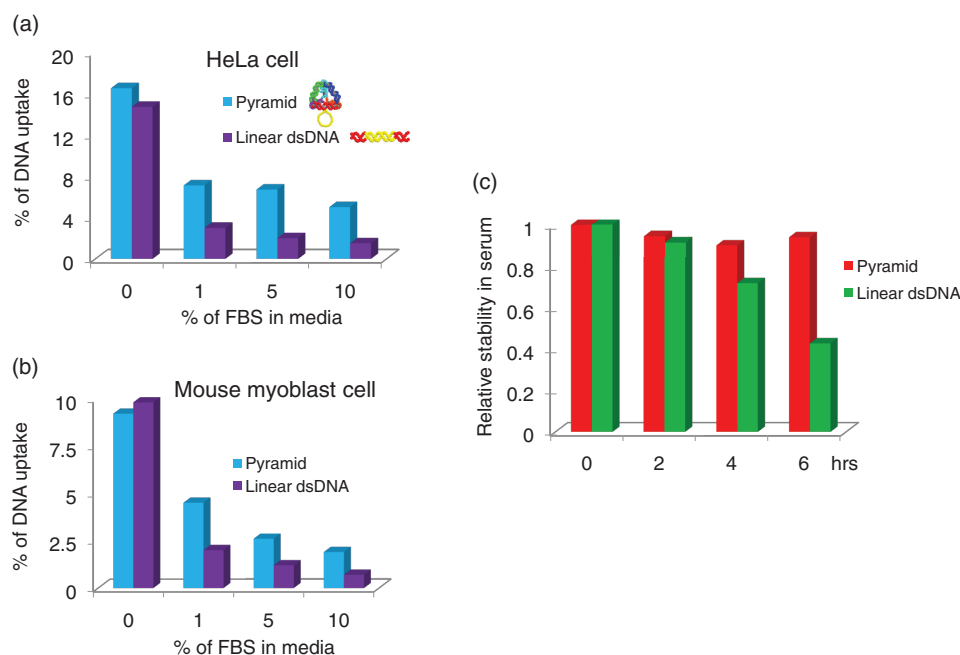


**Figure 3.** Effect of fetal bovine serum (FBS) concentration on DNA uptake in a) HeLa cells and b) C2C12 mouse myoblast cells. All DNA forms bearing Cy5 labels were incubated with each cell type for 5 h and analyzed by flow cytometry. c) Stability of various DNA–lipofectamine mixtures in the presence of 10% serum. The plot was generated from quantification of band intensities in a denaturing gel, after incubation in 10% serum for the indicated times.

require the removal of free hydroxyls (i.e., ligation). While chemical or enzymatic ligation can improve the serum stability of traditional DNA forms,<sup>[24]</sup> it can also have the undesired result of reducing antisense activity.<sup>[25]</sup>

To demonstrate *intracellular* antisense activity, DNA pyramids were incubated with C2C12 cells constitutively expressing EGFP. It is well known that to modulate gene expression inside cells, a delivery vehicle must overcome several barriers, including uptake, transport, localization.<sup>[19]</sup> For comparison with pyramids, the antisense strand was hybridized along its “arms,” resulting in a partial duplex: linear dsDNA displaying the single-stranded antisense loop as shown in the inset of **Figure 4a**. All samples were mixed with lipofectamine and incubated for 24 h in media containing 10% serum. Both Cy5 and EGFP signals (Figure S5, SI) were monitored with flow cytometry, so as to simultaneously determine cellular uptake and protein expression levels. In the presence of 10% serum, pyramids showed higher uptake than the corresponding partial duplex, reflected by the peak shift in Figure 4a. Specifically, levels of DNA uptake were 22.5% for pyramids and 10.1% for partial duplex DNA (Figure 4b, purple). As mentioned above, the increased uptake of pyramids is a direct consequence of their enhanced resistance to nucleases. This improved uptake of pyramids consequently leads to more effective inhibition of EGFP. To quantitate these experiments, we use the *reduction* in EGFP levels, with the untreated controls set at a level of 0%. For samples treated with antisense pyramids, the reduction was approximately 40%, and is significantly better than treatment with partial duplexes (Figure 4b, blue). Importantly, at these doses there was no detectable toxicity due to any of the various treatments (Table S1, SI). The

difference between uptake and gene silencing is presumably due to various intracellular barriers, and will be the subject of future studies. Representative fluorescence images also revealed that incubation with pyramids led to greater down-regulation of EGFP expression, as compared to untreated or partial duplex DNA (Figure 4c). Considering that most *in vitro* transfection studies are conducted in serum-free media (or with heat-inactivated serum), the improved stability of antisense pyramids in the presence of serum is particularly promising for antisense therapeutics.

To move beyond the proof-of-concept stage, we designed and assembled (Figure S6, SI) an antisense pyramid to target a cancer-relevant protein. The MDM2 protein is over-expressed in many human cancers and is a negative regulator of the p53 tumor suppressor protein.<sup>[26]</sup> Depicted schematically in Figure 4d, MDM2 and p53 interact through auto-regulatory feedback loop: MDM2 is transcriptionally activated by p53, and in turn inhibits p53 activity in multiple ways. Accordingly, down-regulation of MDM2 has been recognized as a potential strategy for cancer therapy.<sup>[27]</sup> Treatment of MCF7 human breast cancer cells with our MDM2 antisense pyramids resulted in a significant reduction of MDM2 protein compared to partial duplexes, as determined by Western blotting (Figure 4e). These results demonstrate that antisense DNA pyramids are capable of modulating a therapeutically important protein target.

### 3. Conclusion

We have designed, assembled and demonstrated the antisense capabilities of self-assembled DNA nanostructures.

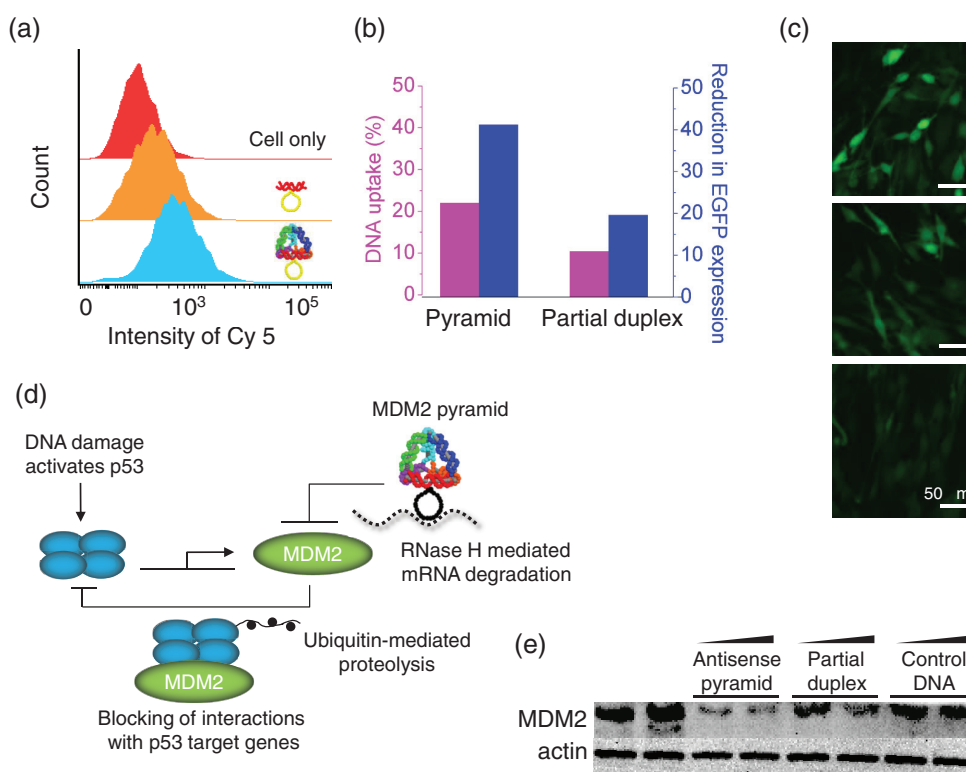


**Figure 4.** a) Flow cytometry of EGFP-expressing C2C12 cells after 24 h, following: no treatment, with partial duplex, and with antisense pyramid. b) Quantification of cell uptake and reduction of EGFP expression, as obtained by flow cytometry. c) Representative fluorescence microscopy of EGFP-expressing C2C12 cells, from top to bottom: no treatment, with partial duplex, with antisense pyramid. d) Schematic of autoregulatory feedback loop between p53 and MDM2, including the mode of antisense pyramid regulation. e) Western blot of MDM2 protein levels in MC7 cells with (from left to right): no treatment, with antisense pyramid, with partial duplex, with control DNA (strand 5). In all but the first case, both low and high doses are tested. See experimental section in the SI.

Under (cell-free) *in vitro* conditions, degradation of mRNA and inhibition of protein expression demonstrated that antisense pyramids can achieve specific gene modulation. The stability of these pyramids with respect to degradation by nucleases led to improved uptake and antisense-mediated gene knockdown in mammalian tumor cells. Our strategy is in marked contrast to conventional nonviral gene delivery, which typically involves either developing artificial “vectors”<sup>[28]</sup> or chemically modifying the nucleic acid itself.<sup>[29]</sup> Since both of the above strategies employ non-natural molecules, unwanted side effects such as toxicity do occur, reducing their usefulness as therapeutics. DNA nanostructures provide an alternative strategy to achieving biological activity. Compared to traditional DNA constructs, these nanostructures have a *simultaneous* array of desirable features: robustness to thermal and mechanical stresses;<sup>[17,18]</sup> multivalent presentation of ligands (Figure 1d); ability for regulation of activity (Figure 2c); resistance to enzymatic degradation (Figure 3c); protein down-regulation (Figure 4b,e); and potential delivery of encapsulated cargo.<sup>[7]</sup>

There is great room for further improvement on these first-generation antisense DNA nanostructures through the use of evolutionary techniques.<sup>[30]</sup> The numerous available approaches to chemically functionalize DNA also increase the scope of this delivery concept.<sup>[31]</sup> In particular, the introduction of both cell-targeting and cell-penetrating

motifs should be readily accomplished, with the latter ideally eliminating the need for the condensing agents used in this study. We envision that the responsive character of DNA nanostructures can be additionally exploited: by responding to thermodynamically favorable binding partners<sup>[17–32]</sup> or environmental stimuli,<sup>[2,33]</sup> changes in the size and/or shape of DNA nanostructures can potentially navigate complex biological obstacles to achieve desirable therapeutic outcomes.

## 4. Experimental Section

**Materials, Assembly, and Characterization:** All oligonucleotides were purchased from Integrated DNA Technology and used without further purification. Stoichiometric quantities of the component DNA strands were mixed in TM buffer (10 mM Tris, 5 mM MgCl<sub>2</sub>) to a final total concentration of 0.5 μM. Solutions were heated at 95 °C for 10 min, followed by step-wise cooling of 60 °C for 1 h, 30 °C for 1 h, and finally to 4 °C using a thermocycler (Bio-Rad). Hybridization between component DNA strands was analyzed with 5% native polyacrylamide gel electrophoresis at 4 °C. For TEM images, 5'-thiol modified DNAs were used for the assembly with 2 nm gold nanoparticles. Thiol-modified strand 1, 3, 4, 5, and unmodified strand 2 were assembled first and stoichiometric quantities of gold nanoparticles were added to the mixture afterwards so that

each pyramid could recruit one particle at each vertex. The gold–DNA mixture was further incubated at room temperature for 2 days with stirring. TEM images were acquired on a JEOL 7C operating at 80 keV. For DLS, samples were passed through a 0.2  $\mu\text{m}$  filter, data were collected with a Malvern Zetasizer Nano ZS, and analyzed by the CONTIN method.

**Cell-Free Protein Down-Regulation:** A standard reaction mixture was used for cell-free protein synthesis reactions.<sup>[34]</sup> Analysis of transcript in cell-free reaction was conducted by withdrawal of 5  $\mu\text{L}$  at each time point and subsequent extraction using a commercial kit (RNeasy Mini, Qiagen). For specific regulation of gene expression, pyramid or partial duplex (0.12  $\mu\text{M}$ ) and anti-antisense oligonucleotide (0.24  $\mu\text{M}$ ) were used. The size of the cell-free synthesized protein was analyzed by 15% SDS-PAGE. Fluorescence of expressed EGFP was monitored as the cell-free reaction was conducted in 96-well plates on a fluorescence spectrophotometer (Varioskan Flash, Thermo Scientific). The fluorescence intensity of EGFP was measured at 30 °C.

**Cellular Uptake:** Fluorescently labeled pyramids were formed by incorporating a Cy5-modified strand 2 and stepwise cooling described above. Either pyramid or partial duplex (1  $\mu\text{g}$ ) were mixed with Lipofectamine 2000 (4  $\mu\text{L}$ ) (Invitrogen) diluted in media (100  $\mu\text{L}$ ) and incubated for 20 min at room temperature. The resulting complexes were incubated with  $10^5$  HeLa cells (ATCC) for 5 h in the different concentrations of FBS (ATCC) in culture media, with a final DNA concentration of 42 nM. All samples were analyzed with a BD LSR II (BD Biosciences) flow cytometer.

**Intracellular Down-Regulation:** C2C12 cells that stably express EGFP (gift from T. Emrick, UMass) were seeded at 25 000 cells/well into 12-well plates (Becton Dickinson) at 24 h prior to transfection and grown with appropriate antibiotics. A mixture of EGFP antisense pyramid and lipofectamine 2000 was added to media containing 10% FBS and incubated with cells, with a final DNA concentration of 42 nM. After 24 h, transfected cells were washed, removed by trypsinization and resuspended in 500  $\mu\text{L}$  of fluorescence-activated cell sorting (FACS) running buffer (5% FBS in PBS). Uptake of Cy5-labeled antisense pyramid and EGFP expression were monitored at the same time using a BD LSR II (BD Biosciences) flow cytometer. Analysis was performed with FlowJo (Tree Star), using untransfected cells as the negative control. Gating was performed such that the negative controls had 5% positive events. Fluorescence images of transfected cells were obtained with an Olympus IX71 inverted microscope (under identical magnification and exposure settings) and analyzed with ImageJ software.

MCF7 cells were incubated with low dose (1  $\mu\text{g}$ ) or high dose (2  $\mu\text{g}$ ) of MDM2 antisense pyramids or partial duplexes in the presence of lipofectamine 2000, as described above. After 48 h, cells were lysed with CellLytic M (Sigma), were fractionated by SDS PAGE and transferred to polyvinylidene fluoride (PVDF) transfer membrane (Millipore). The membrane was incubated with Roche blocking solution for 1 h. Subsequently, the membrane was incubated with primary antibody (anti-MDM2, Santa Cruz biotechnology or anti- $\beta$ -actin, Abcam) overnight at 4 °C. Goat antimouse IgG-horse radish peroxidase conjugated antibody (Abcam) was added to the membrane and proteins were detected using chemiluminescence reagents from Amersham. Detection was performed on a Kodak imaging station.

## Supporting Information

Supporting Information is available from the Wiley Online Library or from the author.

## Acknowledgements

We thank the following individuals for their assistance: S. Pelkar (C2C12 experiments), L. Ramos-Mucci (sequence design), Y. Jeong (TEM imaging), and D. Greene (DLS analysis). We also thank the NSF MRSEC (DMR-0820506) and R. Fissore for use of their facilities. This work was financially supported by an NSF CAREER Award (DMR-0847558) to H.B., and the NSF Center for Hierarchical Manufacturing (CMMI-1025020).

- [1] a) J. D. Watson, F. H. Crick, *Nature* **1953**, *171*, 737–738; b) N. C. Seeman, *Ann. Rev. Biochem.* **2010**, *79*, 65–87.
- [2] a) C. Wang, Z. Huang, Y. Lin, J. Ren, X. Qu, *Adv. Mater.* **2010**, *22*, 2792–8; b) C. Mao, W. Sun, Z. Shen, N. C. Seeman, *Nature* **1999**, *397*, 144–146; c) B. Yurke, A. J. Turberfield, A. P. Mills, F. C. Simmel, J. L. Neumann, *Nature* **2000**, *406*, 605–608; d) H. Yan, X. Zhang, Z. Shen, N. C. Seeman, *Nature* **2002**, *415*, 62–65; e) W. Dittmer, A. Reuter, F. Simmel, *Angew. Chem. Int. Ed.* **2004**, *43*, 3550–3553; f) P. W. K. Rothemund, *Nature* **2006**, *440*, 297–302; g) F. A. Aldaye, H. F. Sleiman, *J. Am. Chem. Soc.* **2007**, *129*, 4130–4131; h) D. Lubrich, J. Lin, J. Yan, *Angew. Chem. Int. Ed.* **2008**, *47*, 7026–7028; i) E. S. Andersen, M. Dong, M. M. Nielsen, K. Jahn, R. Subramani, W. Mamdouh, M. M. Golas, B. Sander, H. Stark, C. L. P. Oliveira, J. S. Pedersen, V. Birkedal, F. Besenbacher, K. V. Gothelf, J. Kjems, *Nature* **2009**, *459*, 73–6; j) O. I. Wilner, Y. Weizmann, R. Gill, O. Lioubashevski, R. Freeman, I. Willner, *Nat. Nanotechnol.* **2009**, *4*, 249–54.
- [3] F. Eckstein, *Expert Opin. Biol. Ther.* **2007**, *7*, 1021–34.
- [4] J.-W. Keum, H. Bermudez, *Chem. Commun.* **2009**, 7036–7038.
- [5] a) M. E. Hogan, M. W. Roberson, R. H. Austin, *Proc. Natl. Acad. Sci. USA* **1989**, *86*, 9273–9277; b) D. Shore, J. Langowski, R. L. Baldwin, *Proc. Natl. Acad. Sci. USA* **1981**, *78*, 4833–4837.
- [6] S. Ko, H. Liu, Y. Chen, C. Mao, *Biomacromolecules* **2008**, *9*, 3039–3043.
- [7] C. M. Erben, R. P. Goodman, A. J. Turberfield, *Angew. Chem. Int. Ed.* **2006**, *45*, 7414–7417.
- [8] C. Teller, I. Willner, *Curr. Opin. Biotechnol.* **2010**, *21*, 376–91.
- [9] R. P. Goodman, I. A. T. Schaap, C. F. Tardin, C. M. Erben, R. M. Berry, C. F. Schmidt, A. J. Turberfield, *Science* **2005**, *310*, 1661–1665.
- [10] S. Williams, K. Lund, C. Lin, P. Wonka, S. Lindsay, H. Yan, *DNA Computing: 14th International Meeting on DNA Computing*, Vol. 5347, 1st ed., Springer, New York **2009**.
- [11] A. J. Mastroianni, S. A. Claridge, A. P. Alivisatos, *J. Am. Chem. Soc.* **2009**, *131*, 8455–9.
- [12] H. Wu, W. F. Lima, S. T. Crooke, *J. Biol. Chem.* **1999**, *274*, 28270–8.
- [13] a) C. F. Bennett, E. E. Swayze, *Annu. Rev. Pharmacol. Toxicol.* **2010**, *50*, 259–93; b) N. K. Sahu, G. Shilakari, A. Nayak, D. V. Kohli, *Curr. Pharm. Biotechnol.* **2007**, *8*, 291–304.
- [14] Y. Shao, Y. Wu, C. Y. Chan, K. McDonough, Y. Ding, *Nucleic Acids Res.* **2006**, *34*, 5660–9.
- [15] J.-W. Keum, J.-H. Ahn, T. J. Kang, D.-M. Kim, *Biotechnol. Bioeng.* **2009**, *102*, 577–582.

- [16] J. R. Swartz, *Curr. Opin. Biotechnol.* **2001**, *12*, 195–201.
- [17] R. P. Goodman, M. Heilemann, S. Dooset, C. M. Erben, A. N. Kapanidis, A. J. Turberfield, *Nat. Nanotechnol.* **2008**, *3*, 93–96.
- [18] D. G. Greene, J.-W. Keum, H. Bermudez, unpublished.
- [19] T. Segura, L. D. Shea, *Annu. Rev. Mater. Res.* **2001**, *31*, 25–46.
- [20] a) P. S. Eder, R. J. DeVine, J. M. Dagle, J. A. Walder, *Antisense Res. Dev.* **1991**, *1*, 141–51; b) B. P. Monia, J. F. Johnston, H. Sasmor, L. L. Cummins, *J. Biol. Chem.* **1996**, *271*, 14533–40.
- [21] M. Lu, Q. Guo, N. C. Seeman, N. R. Kallenbach, *J. Biol. Chem.* **1989**, *264*, 20851–20854.
- [22] Q. Mei, X. Wei, F. Su, Y. Liu, C. Youngbull, R. Johnson, S. Lindsay, H. Yan, D. Meldrum, *Nano Lett.* **2011**, *11*, 1477–1482.
- [23] D. Suck, *Biopolymers* **1997**, *44*, 405–421.
- [24] D. A. Di. Giusto, G. C. King, *J. Biol. Chem.* **2004**, *279*, 46483–46489.
- [25] X. Tang, M. Su, L. Yu, C. Lv, J. Wang, Z. Li, *Nucleic Acids Res.* **2010**, *38*, 3848–55.
- [26] L. T. Vassilev, *Trends Mol. Med.* **2007**, *13*, 23–31.
- [27] a) S. Agrawal, *Biochim. Biophys. Acta* **1999**, *1489*, 53–68; b) H. Wang, L. Nan, D. Yu, S. Agrawal, R. Zhang, *Clin. Cancer Res.* **2001**, *7*, 3613–24.
- [28] a) D. W. Pack, A. S. Hoffman, S. Pun, P. S. Stayton, *Nat. Rev. Drug Discov.* **2005**, *4*, 581–93; b) D. Putnam, *Nat. Mater.* **2006**, *5*, 439–51.
- [29] M. A. Behlke, *Oligonucleotides* **2008**, *18*, 305–319.
- [30] A. D. Ellington, J. W. Szostak, *Nature* **1992**, *355*, 850–2.
- [31] S. Verma, F. Eckstein, *Annu. Rev. Biochem.* **1998**, *67*, 99–134.
- [32] M. M. Maye, M. T. Kumara, D. Nykypanchuk, W. B. Sherman, O. Gang, *Nat. Nanotechnol.* **2010**, *5*, 116–20.
- [33] S. Modi, S. M. G. D. Goswami, G. D. Gupta, S. Mayor, Y. Krishnan, *Nat. Nanotechnol.* **2009**, *4*, 325–30.
- [34] J.-H. Ahn, H.-S. Chu, T.-W. Kim, I.-S. Oh, C.-Y. Choi, G.-H. Hahn, C.-G. Park, D.-M. Kim, *Biochem. Biophys. Res. Commun.* **2005**, *338*, 1346–52.

Received: September 1, 2011  
Published online: October 25, 2011